ISSN 1062-8738, Bulletin of the Russian Academy of Sciences: Physics, 2023, Vol. 87, No. 6, pp. 692–696. © Allerton Press, Inc., 2023.
Russian Text © The Author(s), 2023, published in Izvestiya Rossiiskoi Akademii Nauk, Seriya Fizicheskaya, 2023, Vol. 87, No. 6, pp. 786–791.

Effect of Microstructure on the Thermoelectromotive Force of a Thermoelectric Composite of the Bi_2Te_3 (Matrix) + *x*Ni (Filler) System

M. Zhezhu[a, *], A. E. Vasil'ev[b], and O. N. Ivanov[a, b]

[a] *Belgorod State Technological University, Belgorod, 308012 Russia*
[b] *Belgorod State University, Belgorod, 308015 Russia*
**e-mail: marina_jeju@mail.ru*

Received December 5, 2022; revised December 23, 2022; accepted February 27, 2023

Abstract—Patterns are found in the effect the content of a ferromagnetic filler has on features of the microstructure of Ni core–shell $NiTe_2$ inclusions, changes in the Seebeck coefficient, and concentration of electrons in samples of the Bi_2Te_3 (matrix) + *x*Ni (filler) composites with $x = 0.00$; 0.50; 0.85; 1.25 and 1.50 wt %. It is shown that the Seebeck coefficient in composites with $x = 0.50$ and 0.85 exceeds the calculated values, due possibly to additional scattering of electrons by the magnetic moments of inclusion atoms.

DOI: 10.3103/S1062873823701927

INTRODUCTION

Thermoelectric generators, which directly convert heat to electrical energy due to the Seebeck effect, are used for supplying power to such hard-to-reach consumers as craft for studying deep space and stations for the anti-corrosion protection of gas pipelines. Their efficiency depends on the properties of the materials that are used, including the Seebeck coefficient. The growth of the Seebeck coefficient raises the thermoelectric Q-factor of the material. It is known that a specific defect structure must form in the material to increase the Q-factor [1–3]. Intentionally created defects of different natures, sizes, and dimensions are centers of scattering for both electrons and phonons. Electron scattering affects the electrical conductivity and thermo EMF of a thermoelectric material, while phonon scattering determines the contribution from the lattice to its total thermal conductivity. In composites (nanocomposites) consisting of a matrix based on a thermoelectric material and filler of a different nature, filler inclusions randomly or regularly distributed throughout the matrix volume act as efficient centers of electron and phonon scattering. Materials with magnetoactive inclusions (Ni, Fe, Co, and Gd) whose atoms have magnetic moments, are promising thermoelectric composites [4–8]. Additional electron scattering at atomic magnetic moments can occur in such composites. It was shown earlier by the example of a thermoelectric composite consisting of a $Bi_{0.37}Sb_{1.63}Te_3$ matrix with $GdCo_2$ magnetoactive inclusions that such additional scattering can raise the thermo EMF of the composite (expressed as the Seebeck coefficient) and thus increase the thermoelectric Q-factor of the composite [9].

The aim of this work was to reveal possible increases in the thermo EMF (Seebeck coefficient) in Bi_2Te_3 (matrix) + Ni (filler) composites with different filler contents. The bismuth telluride chosen as the matrix is used as a component of Bi_2Te_3–Bi_2Se_3 and Bi_2Te_3–Sb_2Te_3 solid solutions with *n*- and *p*-type conductivities, respectively. These solid solutions are widely used in low-temperature thermoelectric power generators and solid-state refrigerators [10].

EXPERIMENTAL

Bi_2Te_3 and Ni powders were synthesized in order to obtain Bi_2Te_3 + *x*Ni (x= 0.00, 0.50, 0.85, 1.25, and 1.50 wt %) composites. Bi_2O_3 and TeO_2 (high purity grade) dissolved in ethylene glycol were used as the initial reagents to synthesize the Bi_2Te_3 powder. KOH alkali agent was added to the solution to control its pH values. The resulting solution was transferred to a flask and boiled to evaporate its water. The flask was then hermetically sealed with a reflux condenser and kept for 4 h at 458 K. The obtained suspension was cooled to room temperature. The synthesized powder was separated via filtration, purified by washing 3 times with ethanol and acetone, and dried for 2h in an argon atmosphere at 523 K. To synthesize the Ni powder, $Ni(NO_3)\cdot 6H_2O$ (5 g) was dissolved in ethylene glycol (400 mL) and KOH (10 g) was added to the resulting solution. The reaction mixture was heated to 353 K with intense stirring to reach a homogeneous state.

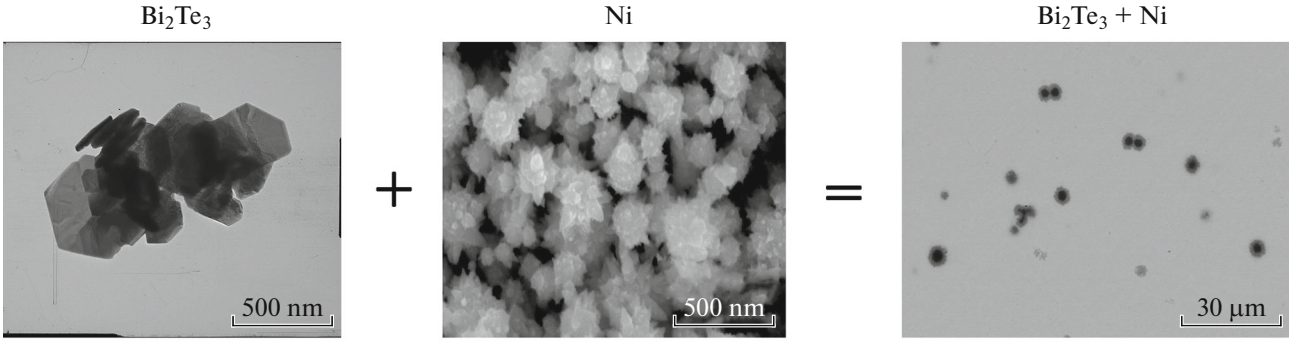

Fig. 1. Scheme of formation of the matrix–filler microstructure in our Bi_2Te_3 + 0.5 wt % Ni composite during the spark plasma sintering of the initial powder of Bi_2Te_3 (matrix material) and Ni (filler material). Typical particles of the matrix and filler powders are given in the corresponding SEM images. The BSE image (right) of the polished composite surface visualizes dark grey inclusions of the filler distributed over the light grey matrix by means of compositional contrast (shades of gray).

The obtained sol was cooled to room temperature and hydrazine hydrate was added slowly. The mixture was then heated to 373 K at held for 1 h to complete the $Ni^{2+} \rightarrow Ni^0$ reduction. The obtained Ni powder was collected using a neodymium magnet and rinsed with ethanol and acetone to remove organic impurities. To prepare composites, Bi_2Te_3 and Ni powders were taken in a stoichiometric ratio corresponding to a certain x value and mixed thoroughly for 30 min using a planetary ball mill. The mixture was treated for 2 min via spark plasma sintering using the SPS 25/10 system (Thermal Technology, United States) at a pressure of 40 MPa and a temperature of 573 K. Scanning electron microscopy (SEM) was used to study features of the composite's microstructure using a Nova NanoSEM 450 microscope (Thermo Fisher Scientific, United States). To reveal the features of the phase distribution of the matrix and filler components of the composite, SEM images were obtained in the backscattered electron (BSE) mode. Seebeck coefficient S (thermo EMF coefficient or thermal EMF) of composites was measured by differentially using a ZEM-3 (ULVAC GmbH, Germany) electric resistance measuring system. The concentration of electrons in composites with different contents of filler was determined by studying the Hall effect with a Mini Cryogen Free (Cryogenic Ltd, United Kingdom) magnet system.

RESULTS AND DISCUSSION

Figure 1 shows the scheme of the formation of the desired matrix–filler microstructure in $Bi_2Te_3 + x$Ni composites after spark plasma sintering of the initial powders of the matrix and filler materials for a composite with $x = 0.50$ wt %. The left part of Fig. 1 contains SEM images of typical particles for the Bi_2Te_3 and Ni initial powders. The initial Bi_2Te_3 powder had the $R3m$ space symmetry group with crystal lattice parameters of $a = 0.4354$ nm and $c = 3.035$ nm and consisted mainly of hexagonal plates with an average size of several hundred nanometers and a thickness of ~100 nm. The initial Ni powder had the $Fm3m$ face-centered cubic structure with crystal lattice parameters of $a = 0.3525$ nm and consisted of agglomerated particles of almost spherical shape with diameters of 150–200 nm. Agglomerates consisted of individual particles of irregular shape with a size of several tens of nanometers (i.e., the initial Ni powder consisted of multiparticle structures). The agglomeration of individual Ni particles into spherical structures during the synthesis of the initial powder could have been due to ferromagnetic interaction (the Curie temperature of Ni is 628 K). The right part of Fig. 1 shows the BSE image of the polished surface of the material obtained using Bi_2Te_3 and Ni initial powders. Matrix and filler phases are clearly seen in the BSE image because the phase consisting of atoms with a higher average sequential number reflects a higher number of electrons and lighter areas in the image appear. We can see that the filler inclusions in the studied composite (dark grey regions) were randomly distributed over the light grey matrix. This identification of matrix and filler materials was confirmed earlier via X-ray analysis and studying the elemental compositions of the $Bi_2Te_3 + x$Ni composites [6]. The surface density of filler inclusions (the number of inclusions per area unit) grew along with the content of nickel (Fig. 2). The filler inclusions in composites with different Ni contents have a core–shell structure. As was shown in [6], ferromagnetic Ni is the core of inclusions. At the same time, the shells are a new phase of $NiTe_2$ that forms due to the $Ni^0 + 2Te^{2-} \rightarrow NiTe_2$ chemical reaction between the matrix and the filler during spark plasma sintering and has no ferromagnetic properties. The microstructure of Ni@$NiTe_2$ inclusions can be characterized by shell thickness l and core radius R. By considering the l/R ratio, all inclusions can be divided into three main types. Inclusions of the first type consist of a large core and thin shell (i.e., R (or $\gg$) $> l$. The R and l values are almost equal for inclusions of the

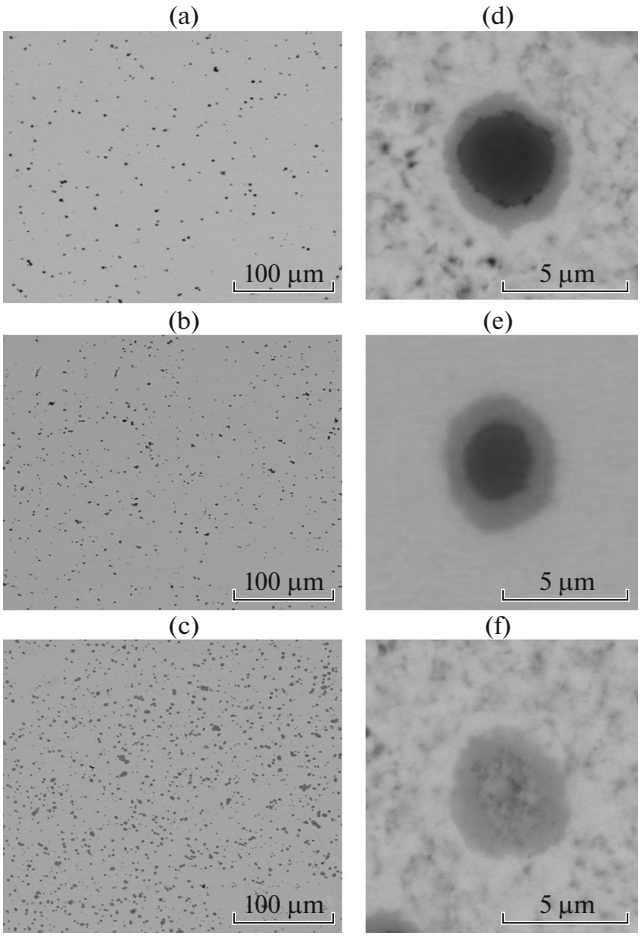

Fig. 2. BSE images of polished surfaces and typical inclusions of $Bi_2Te_3 + x$Ni composite samples with x = (a, d) 0.50, (b, e) 0.85, and (c, f) 1.50.

second type, and the shell predominates among inclusions of the third type (i.e., l (or $\gg$) > R). It was established that when the content of Ni in composites is raised, the inclusions are gradually transformed from the first to the third type though inclusions of the second type. Figure 2 shows BSE images of typical inclusions that confirm this tendency. The core predominates in all Ni core–$NiTe_2$ shell inclusions for the sample with $x = 0.50$ wt %. Inclusions with almost equal sizes of the core and shell formed when $x = 0.85$ wt %, while inclusions consisting of only the shell material predominated when $x = 1.50$ wt %. The primary mechanism of the formation of Ni@$NiTe_2$ inclusions was the high-temperature diffusion redistribution of matrix and filler atoms when synthesizing the composite from the initial powders. It is this diffusion that initiates the $Ni^0 + 2Te^{2-} \rightarrow NiTe_2$ chemical reaction. The rise in the shell fraction and the corresponding drop in the core fraction in inclusions of $Bi_2Te_3 + x$Ni composites as the content of Ni grows testifies to diffusion being activated during spark plasma sintering (i.e., higher coefficients of diffusion). However, the temperature and duration of the spark plasma sintering were the same for powders with different contents of Ni. It is therefore logical to assume the coefficient of diffusion is independent of x. To explain the observed changes in inclusion microstructures, we considered the physical mechanisms that operate in spark plasma sintering with the simultaneous action of uniaxial pressure and pulsed electric current on the sintered powder. It is known that the effect of several electrical, mechanical, and temperature factors must be considered [11]. Sintering is initiated under the effect of pulses of electric current passing through particles of the sintered powder that are under constant mechanical pressure. Through the release of Joule heat, compressed particles are heated at contact points because of repeated spark discharges acting in the gaps between contacting particles, resulting in faster thermally activated diffusion of atoms of the sintered material. The specific electrical resistance of Ni and Bi_2Te_3 differs considerably. At room temperature, the specific resistance of Ni is ~6.5×10^{-2} μΩ m [12], while the specific resistance of Bi_2Te_3 used for $Bi_2Te_3 + x$Ni composites is ~23 μΩ m [7]. Introducing Ni into Bi_2Te_3 therefore results in substantial electrical inhomogeneity of the composite. The spatial distribution of electrical inhomogeneities redistributes the electric current so that it flows primarily through areas with less resistance (i.e., through Ni inclusions) [13]. The number of such inclusions grows upon raising the content of Ni, so a large part of the pulsed current flows through inclusions and heats them in places, thereby raising the coefficient of Ni diffusion in the Bi_2Te_3 matrix. The $Ni^0 + 2Te^{2-} \rightarrow NiTe_2$ reaction is accelerated, resulting in experimentally observed growth of the shell fraction in Ni@$NiTe_2$ inclusions.

Figure 3a shows temperature dependences of the Seebeck coefficient of $Bi_2Te_3 + x$Ni composites with different contents of Ni obtained in the 290–550 K range of temperatures. The negative sign of S indicates electrons were the primary charge carriers in the samples. These dependences are typical of Bi_2Te_3-based compounds [14, 15]. A maximum at ~400 K is observed in all $S(T)$ curves. The growth of $S(T)$ observed upon an increase in temperatures below the maximum temperature corresponds to the thermo EMF behavior typical of degenerate electron semiconductors in which the concentration of electrons is virtually independent of temperature. Above the maximum temperature, the Seebeck coefficient falls as the temperature rises, due to the emergence of intrinsic conductivity accompanied by the thermal generation of electron hole pairs. Since the sign of the S of holes is positive, the Seebeck coefficient gradually falls as the temperature rises. We can see the $S(T)$ dependences were affected by the content of Ni. However, this effect on the thermo EMF was complex, due possibly to the simultaneous and interconnected effects of

several mechanisms (e.g., a change in the concentration of electrons; a change in the concentration, size, and microstructure of Ni core–$NiTe_2$ shell inclusions; and a change in the degree of texturing) on the thermo EMF.

To specify the effect the ferromagnetic filler had on the thermo EMF of $Bi_2Te_3 + x$Ni composites with different x, we used an approach proposed earlier to analyze the effect $GdCo_2$ inclusions had on the thermo EMF of $Bi_{0.37}Sb_{1.63}Te_3$ [9]. To do so, we must know the change in concentration n of electrons in composites upon a change in the content of filler. Dependence $n(x)$ obtained by studying the Hall effect at room temperature is shown in the insert in Fig. 3b. This dependence had a maximum at $x = 0.85$ wt %. The metallic Ni in the inclusions obviously acted as the source of electrons in the composites. On the one hand, the content of Ni in the initial powders of the filler grew when x was raised, which should have increased n in composites. On the other hand, the fraction of Ni cores in Ni@$NiTe_2$ fell when the composites were sintered (Fig. 2), which should have reduced n. In other words, the fraction of metal Ni in these inclusions fell despite the growth of filler inclusions upon raising n. A maximum appeared in the $n(x)$ dependence, due to the competing action of these factors.

We assume that S and n are related through the expression

$$S = \frac{2k_B^2 T m^*}{3e\hbar^2}\left(\frac{\pi}{3n}\right)^{2/3}\left(\frac{3}{2} + \gamma\right), \quad (1)$$

where k_B is Boltzmann constant, T is the absolute temperature, e is the electron charge, $\hbar$ is the Planck constant, m^* is effective electron mass, and γ is the scattering factor.

The effective electron mass of pure (without filler) Bi_2Te_3 was calculated according to a model of a simple parabolic zone using the equation

$$n = 4\pi\left(\frac{2m^* k_B T}{h^2}\right)^{3/2} F_{1/2}(\eta), \quad (2)$$

where $F_{1/2}(\eta)$ is Fermi integral for the conduction band and η is the reduced Fermi level.

The $S(T)$ experimental dependence was then used to determine the value of the Fermi integral. According to calculations using Eq. (2) with $F_{1/2}(\eta) = 1.6487$ and $T = 300$ K, the m^* value was $0.94m_e$ (where m_e is free electron mass). Figure 3b shows the $|S| = f(n)$ dependence built with Eq. (1) using this value of the effective electron mass and experimental values of the Seebeck coefficient measured at room temperature on $Bi_2Te_3 + x$Ni samples with different Ni contents and n values (the symbols for different x correspond to the ones used in Fig. 3a). We can see the Seebeck coefficients of samples with $x = 0.00$, 1.25, 1.50 wt % are in good agreement with the calculated $|S| = f(n)$ curve

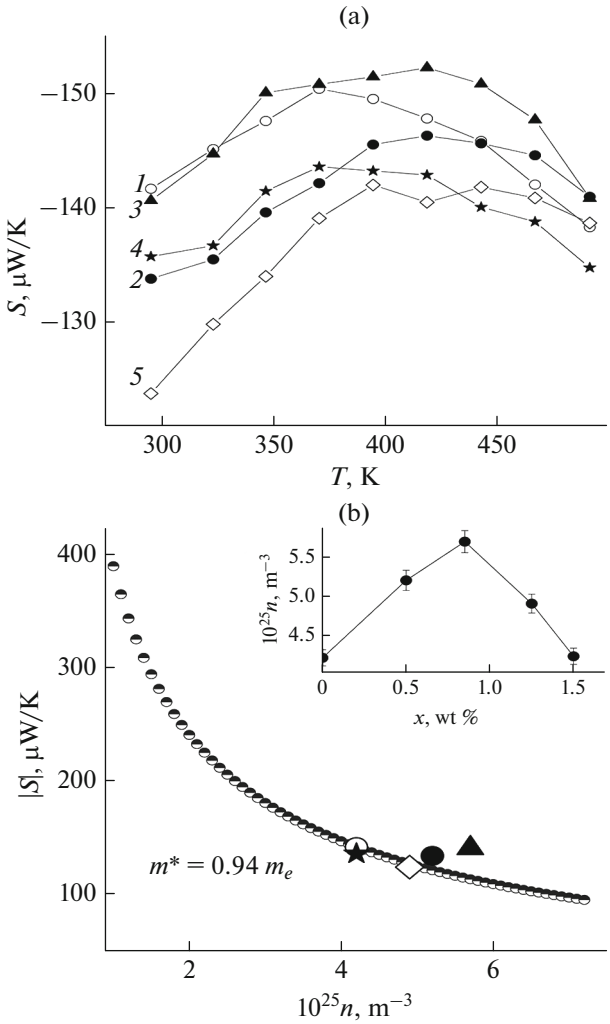

Fig. 3. (a) Temperature dependences of the Seebeck coefficient of $Bi_2Te_3 + x$Ni composite samples with x = (*1*) 0.00, (*2*) 0.50, (*3*) 0.85, (*4*) 1.25, and (*5*) 1.50. (b) Dependence of the Seebeck coefficient on the concentration of electrons at 300 K calculated for $m^* = 0.94m_0$. The symbols show the experimental values of S for samples of $Bi_2Te_3 + x$Ni composite with different contents of Ni (the symbols for different x correspond to those of the curves in Fig. 3a). The inset shows the dependence of the concentration of electrons on the content of Ni.

while the $|S|$ values of samples with Ni contents of 0.50 and 0.85 wt % are slightly higher. Such deviation of the experimental values from those calculated could indicate the emergence of a complementary mechanism of electron scattering in composites with this content of nickel. This mechanism could raise the Seebeck coefficient through an increase in scattering factor γ in Eq. (1). It should be noted that no inclusions were observed in the sample with $x = 0.00$ wt %. When $x =$ 1.25 and 1.50 wt %, samples contained numerous inclusions with $NiTe_2$ shells predominating rather than ferromagnetic Ni cores. Inclusions with predom-

inantly Ni cores existed only in samples with $x = 0.50$ and 0.85 wt %. The concentration of electrons grew at these contents of Ni; i.e., metal Ni cores effectively work as a source of dopant. We may conclude that the scattering of electrons on the magnetic moments of Ni atoms in the composition of the cores of Ni@$NiTe_2$ inclusions is a complementary mechanism of electron scattering that raises the values of the Seebeck coefficient in composites with Ni contents of 0.50 and 0.85 wt %.

CONCLUSIONS

The thermo EMF of $Bi_2Te_3 + x$Ni composites with a certain content of filler can grow due to the scattering of electrons on the magnetic moments of Ni atoms in the cores of Ni core–$NiTe_2$ shell inclusions. Samples with different fractions of cores and shells in inclusions can be obtained by changing the content of Ni, and such samples have different efficiencies of electron scattering.

FUNDING

This work was supported by the RF Ministry of Science and Higher Education, project no. 0625-2020-0015.

CONFLICT OF INTEREST

The authors declare that they have no conflicts of interest.

REFERENCES

1. Saito, W., Hayashi, K., Dong, J., et al., *Sci. Rep.*, 2020, vol. 10, p. 2020.
2. Dong, X., Cui, W., Liu, W.-D., et al., *J. Mater. Sci. Technol.*, 2021, vol. 86, p. 204.
3. Zhou, C., Lee, Y.K., Cha, J., et al., *J. Am. Chem. Soc.*, 2018, vol. 140, p. 9282.
4. Zhao, W., Liu, Z., Wei, P., et al., *Nat. Nanotechnol.*, 2017, vol. 12, p. 55.
5. Zhao, W., Liu, Z., Sun, Z., et al., *Nature*, 2017, vol. 13, p. 247.
6. Ivanov, O., Yaprintsev, M., Vasil'ev, A., et al., *Chin. J. Phys.*, 2022, vol. 77, p. 24.
7. Ivanov, O.N., Yapryntsev, M.N., Vasil'ev, A.E., et al., *Glass Ceram.*, 2022, vol. 78, p. 442.
8. Ivanov, O.N., Yapryntsev, M.N., Vasil'ev, A.E., et al., *Glass Ceram.*, 2022, vol. 79, p. 180.
9. Li, C., Ma, S., Cui, W., et al., *Mater. Today Phys.*, 2021, vol. 19, p. 100409.
10. Goldsmid, H.J., *Materials*, 2014, vol. 7, p. 2577.
11. Chaim, R., *Mater. Sci. Eng., A*, 2007, vol. 443, nos. 1–2, p. 25.
12. Greig, D., *J. Phys. C*, 1968, vol. 1, p. 1359.
13. Xu, R., Husmann, A., Rosenbaum, T.F., et al., *Nature*, 1997, vol. 390, p. 57.
14. Perera, D., Tokita, M., and Moricca, S., *J. Eur. Ceram. Soc.*, 1997, vol. 18, p. 401.
15. Song, S.-X., Wang, Z., and Shi, G.-P., *Ceram. Int.*, 2013, vol. 39, p. 1393.

Translated by N. Saetova